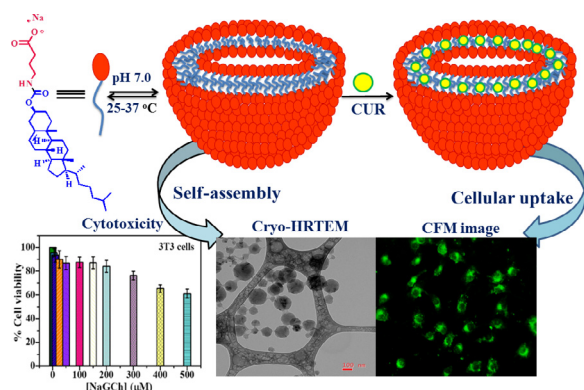


## Regular Article

Spontaneous vesicle formation by  $\gamma$ -aminobutyric acid derived steroidal surfactant: Curcumin loading, cytotoxicity and cellular uptake studiesDeepnath Bajani<sup>a</sup>, Joykrishna Dey<sup>a,\*</sup>, Y. Rajesh<sup>b</sup>, Satyabrata Bandyopadhyay<sup>c</sup>, Mahitosh Mandal<sup>b</sup><sup>a</sup> Department of Chemistry, Indian Institute of Technology Kharagpur, Kharagpur 721 302, India<sup>b</sup> School of Medical Science and Technology, Indian Institute of Technology Kharagpur, Kharagpur 721 302, India<sup>c</sup> TIFR Centre for Interdisciplinary Sciences (TCIS), Tata Institute of Fundamental Research, Hyderabad 500075, India

## GRAPHICAL ABSTRACT



## ARTICLE INFO

## Article history:

Received 17 April 2017

Revised 27 July 2017

Accepted 28 July 2017

Available online 29 July 2017

## Keywords:

Cholesterol

Surfactant

Vesicle

Cytotoxicity

Curcumin

## ABSTRACT

Cholesterol (Chol) is a ubiquitous steroidal component of cell membrane and is known to modulate the packing of phospholipids within the bilayer. Thus, Chol has been frequently used in the formulation and study of artificial “model membranes” like vesicles and liposomes. In this work, we have developed a novel anionic surfactant by conjugating two biomolecules, cholesterol and  $\gamma$ -aminobutyric acid via a urethane linkage. We have studied its physicochemical behavior in aqueous buffer. The surfactant has been shown to spontaneously form small unilamellar vesicles above a very low critical concentration in aqueous neutral buffer at room temperature. The vesicle phase was characterized by use of fluorescence probe, transmission electron microscopy and dynamic light scattering (DLS) techniques. The vesicle bilayer was found to be much less polar as well as more viscous compared to the bulk water. The vesicle stability with respect to change of temperature, pH, and ageing time was investigated by fluorescence probe and DLS techniques. The loading efficiency of the vesicles for the hydrophobic drug, curcumin, was determined and its release under physiological condition was studied. The in vitro cellular uptake of curcumin-loaded vesicles to human breast cancer cell line (MDA-MB-231) also was investigated. The MTT assay showed that the surfactant was non-cytotoxic up to a relatively high concentration.

© 2017 Elsevier Inc. All rights reserved.

\* Corresponding author.

E-mail address: [joydey@chem.iitkgp.ernet.in](mailto:joydey@chem.iitkgp.ernet.in) (J. Dey).

## 1. Introduction

Cancer registers the second leading cause of death in the USA, accounting for nearly 22.5 % of total deaths [1]. Despite gradual downtrend of its mortality rate (22.97% in 2000 and 22.24% in 2014) [1], cancer still continues to hold its rank over the decades. Curcumin, CUR (see Chart 1 for structure), a polyphenol occurring in the herbal remedy and curry spice turmeric (*Curcuma longa*), has been identified as a potential candidate for treating cancer. Its uses are scripted in the ancient Hindu treatise, the *Ayurveda* [2]. The demand of turmeric as a food coloring and flavouring agent is global. The Food and Agriculture Organization of the United Nations records an annual import of over 2400 metric tons of turmeric into the USA for consumer use. In addition to its stimulant and coloring properties in foodstuffs, CUR exhibits a wide range of pharmacological activities, such as antimicrobial, antioxidant, anti-inflammatory, hepato-protective, anti-Alzheimer's, chemopreventive, and chemotherapeutic properties [3–9]. It is well-established that CUR blocks transcriptional factor activator protein-1 (AP-1), nuclear factor-kappaB (NF- $\kappa$ B) [10], and modulates mitogen-activated protein kinase (MAPK) and phosphoinositide-3-kinase-protein kinase B/Akt (PI3 K-PKB/Akt) signalling pathways that could contribute to anti-proliferation and induction of apoptosis in vitro including K562 myelogenous leukemia cells. Further, CUR is a potent inhibitor of three crucial ATP-binding cassette (ABC) drug transporters, such as MDR1, MRP1 and ABCG2, which play a pivotal role in multidrug resistance (MDR) [11,12]. Studies have also reported that CUR inhibited the activity of p210bcR/abl tyrosine kinase in K562 cells [13]. Due to its diverse properties and myriad applications, over 100 chemical and pharmaceutical companies are producing various curcumin products in different forms—from dairy and drinks to tablets and gels—for daily and medical use. Also, various clinical trials are in different phases or have been done to investigate the therapeutic efficacy of CUR [14].

However, the chemistry of CUR is somewhat disappointing. CUR delivery is handicapped by its low water solubility (0.4  $\mu$ g/mL at pH 7.3) as well as its alkaline degradation [15–18]. A simple way to address the solubility and stability issues is to encapsulate it into nano-aggregates, thus protecting it from degradation and metabolism. During the past two decades, extensive research has been on to developing various CUR nanoformulations. Different nanocarriers, such as polymer nanoparticles [19], polymeric micelles [20], liposomes [21], nano-/micro-emulsions [12,22], nanogels [23] solid lipid nanoparticles [24], polymer conjugates [25], have been formulated for the delivery of CUR to tumor cells. Among various nanodelivery systems, vesicles provide an excellent bilayer microenvironment for CUR solubilization. Vesicles that

form spontaneously in aqueous solution and have good long-term stability are even advantageous over liposomes (phospholipid vesicles) as the latter often suffer from instability, poor batch to batch reproducibility, and sterilization difficulties, which limit their application. Kumar et al. have demonstrated enhanced solubilization of CUR in mixed cationic surfactant vesicles [26]. CUR-loaded vesicles formed by nonionic surfactants, such as Tween 80 and F127 in combination with lauric acid and isopropanol showed antimicrobial activity against *Propionibacterium acnes* [27]. Dequalinium-derived cationic vesicles of size 170–200 nm are reported as inhalation formulation with improved stability characteristics and mitochondrial targeting ability for treating acute lung injury [28]. CUR/ $\beta$ -cyclodextrin vesicles are reported to enhance the aqueous solubility of CUR up to 7000 folds, but the vesicles exist in aqueous medium for a month only, showing not-so-good formulation stability [29].

Although there are many reports on liposomal CUR, including two commercially available nanoformulations [30], only a few articles have addressed the chemotherapeutic activity of CUR-loaded vesicles. As a step forward to this direction, in this work we have synthesized a cholesterol-based anionic surfactant, NaGCh (see Chart 1 for structure) and studied its physicochemical behavior in aqueous buffer. In designing NaGCh, two biomolecules, such as cholesterol (Chol) and gamma-amino butyric acid (GABA) were conjugated via a urethane linkage. It is well known that Chol, a typical steroid, is a ubiquitous component of cell membrane and modulates the packing of phospholipids within the bilayer [31]. On the other hand GABA is a four-carbon, non-protein amino acid conserved from bacteria to plants and vertebrates. Although it was discovered in plants long ago [32], but the interest in GABA suddenly moved to animals when it was found that GABA was a chief inhibitory neurotransmitter in the central nervous system. The chemical, physiological, and pharmacological role of GABA have been reviewed in the literature [33,34]. Also, the incorporation of biomolecules like Chol and GABA is expected to render NaGCh cell viable. In a previous paper, we have shown that a structurally similar compound NaChol-Ala, where the amino acid is L-alanine instead of GABA, also formed robust vesicles in aqueous solutions [35]. In the present work, with a wide range of techniques including fluorescence, dynamic light scattering and microscopy, we demonstrate that NaGCh spontaneously forms stable vesicles in neutral buffer at room temperature. These vesicles were investigated for encapsulation and in vitro delivery of CUR to human breast cancer cell line MDA-MB-231. The cytotoxicity and cellular uptake studies were also carried out with the CUR-loaded vesicles.

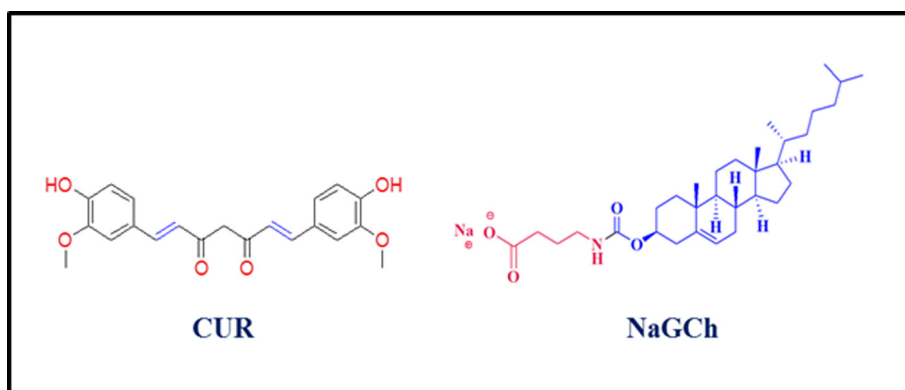


Chart 1. Chemical structure of CUR and NaGCh.

## 2. Results and discussion

### 2.1. Self-assembly studies

#### 2.1.1. Critical aggregation concentration

In aqueous solution, surfactant molecules self-assemble to form aggregates, such as micelles, vesicles, etc. Fluorescence is a powerful and sensitive technique to study the self-assembly properties of surfactants [36–41]. To accurately determine the critical aggregation concentration ( $cac$ ) for the onset of self-assembly formation, we used N-phenyl-1-naphthalamine (NPN) and coumarin-153 (C153) as extrinsic fluorescence probes. We also employed 1,6-diphenyl-1,3,5-hexatriene (DPH) to estimate the fluidity of the microenvironment of the self-assembled aggregates. The hydrophobic probe molecules are poorly soluble in water ( $<1 \mu\text{M}$ ) and have weak fluorescence. But as they are exposed to a nonpolar environment, the fluorescence is enhanced accompanied by a significant blue shift of the emission maximum.

In aqueous buffer (pH 7.0 PBS, 20 mM), NPN alone exhibits a very weak fluorescence with emission maximum ( $\lambda_{\text{max}}$ ) centered at 460 nm. With increasing [NaGCh], the emission maximum was observed to gradually shift toward shorter wavelengths. Also, almost 2.4 times increment in intensity was noted in the presence of NaGCh (see Fig. S1). This clearly suggests that the surfactant molecules self-assemble to form aggregates with a less polar microenvironment, where the probe molecules are preferably solubilized. The variation of relative fluorescence intensity ( $F/F_0$ , where  $F_0$  and  $F$  are the fluorescence intensities in the absence and the presence of the surfactant, respectively) and spectral shift ( $\Delta\lambda = \lambda_{\text{max}}(\text{buffer}) - \lambda_{\text{max}}(\text{sample})$ ) of NPN as a function of [NaGCh] are shown by the plots in Fig. 1. The surfactant concentration corresponding to the onset of the rise of the plots can be taken as its  $cac$  value (Table 1). The  $cac$  value ( $\sim 15 \mu\text{M}$ ) thus obtained is very low. However, the accuracy of the  $cac$  value is further confirmed by the results of fluorescence titration carried out using C153 as a probe molecule (discussed below). The large blue shift ( $\sim 50 \text{ nm}$ ) of the NPN fluorescence suggests that its microenvironments are much less polar than the bulk water.

#### 2.1.2. Shape and size of aggregates

The microstructures of the aggregates were visualized with a transmission electron microscope (TEM). The unstained TEM image of the 0.20 mM (108  $\mu\text{g/mL}$ ) NaGCh dispersion is presented in Fig. 2(a). The micrograph 2a clearly reveals the formation of spherical vesicles having diameter in the range of 20–50 nm. The micrograph 2a also shows clustering of vesicles. An approximate

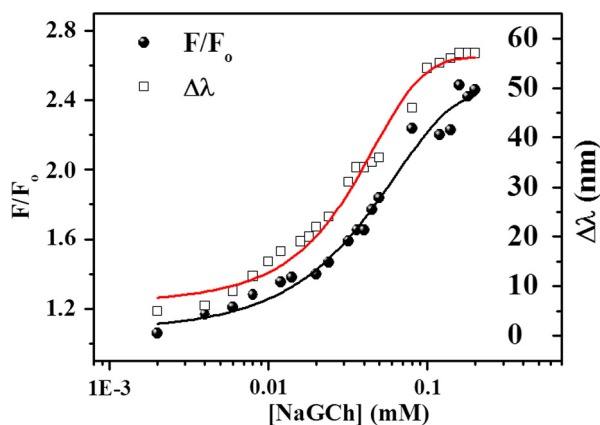


Fig. 1. Variation of relative fluorescence intensity ( $F/F_0$ ) and spectral shift ( $\Delta\lambda$ ) of NPN probe with [NaGCh] at 25 °C.

thickness ( $\sim 4.6 \text{ nm}$ ) of the bilayer vesicle membrane was measured from the TEM image as shown in Fig. 2(a), which is slightly less than twice the length of the Chol moiety of the surfactant. Considering the hydrophobic chain length of NaGCh is equal to 2.53 nm (as obtained by energy minimization studies using Chem-Draw 3D 7.1 software), the membrane is unilamellar one. The small difference ( $\sim 0.46 \text{ nm}$ ) between the values of estimated thickness of the membrane and two times of chain length could be attributed to interdigitation of the hydrocarbon tails in the bilayer membrane. This suggests that NaGCh spontaneously forms small unilamellar vesicles (SUVs) at pH 7. The conventional TEM images are often criticised as artefacts because it involves drying of the samples. Therefore, to confirm vesicle formation in solution, we have performed Cryo-TEM measurement for a representative sample. The micrograph in Fig. 2(b) clearly reveals spherical vesicles of diameters in the range 100–250 nm. However, the size of the vesicles in the Cryo-TEM image is larger than that obtained from conventional TEM. This must be due to drying of the specimen in the latter technique that causes shrinking of the vesicles.

The hydrodynamic diameter ( $d_h$ ) of the vesicles was also obtained by direct measurement using DLS technique. The size distribution histogram (Fig. 2(c)) shows a bimodal distribution profile in PBS (pH 7.0, 20 mM) at 25 °C, suggesting coexistence of small as well as large vesicles in solution which is consistent with the results of Cryo-TEM measurement. The mean  $d_h$  value of the smaller vesicles is ca. 100 nm and that of larger is ca. 500 nm. The presence of large vesicles in solution could be attributed to the oligovesicular clusters formed by localized assembly of the SUVs.

#### 2.1.3. Micropolarity of vesicles

It is well-known that for bilayer aggregates, the packing of the hydrophobic tails is highly ordered and more compact compared to micelles. Thus, the hydrophobic environment of vesicles is likely to be much less polar compared to micellar aggregates. The solvatochromic character of C153 affords a very good correlation between solvent polarity and emission frequency of C153. The micropolarity of the self-assemblies can be expressed in terms of  $\pi^*$ -polarity scale, which is defined by the equation [42]:

$$\bar{\nu}_{em} = 21.217 - 3.505\pi^* \quad (1)$$

where  $\bar{\nu}_{em}$  [in  $10^3 \text{ cm}^{-1}$ ] is the wavenumber corresponding to the emission maximum of C153. In the presence of the surfactant, the emission spectra of C153 showed a maximum at 509 nm, indicating 41-nm blue shift. We used  $\lambda_{em} = 509 \text{ nm}$  to evaluate  $\pi^*$  (Table 1). The calculated  $\pi^*$  value (0.45) corresponds to ethyl acetate solvent. As in the case of NPN, the spectral shifts ( $\Delta\lambda$ ) of C153 were plotted as a function of [NaGCh] (Fig. 3). The  $cac$  value ( $\sim 18 \mu\text{M}$ ) as obtained from the onset of rise of  $\Delta\lambda$  is closely similar to that obtained by fluorescence titration using NPN probe ( $\sim 15 \mu\text{M}$ ), which establishes the accuracy of the measured  $cac$  value.

Like C153, pyrene (Py) is also a highly sensitive polarity probe. Out of five vibronic bands observed in Py emission spectrum, the intensity ratio of the first ( $I_1$ , 374 nm) to the third ( $I_3$ , 384 nm) vibronic band is known to be sensitive to the change in solvent polarity [43]. The  $I_1/I_3$  ratio is termed as the “polarity ratio”. Kalyansundaram et al. [43] reported the polarity ratios for Py monomer in different organic solvents. Normally, high and low values of  $I_1/I_3$  indicate polar and nonpolar environment experienced by Py monomer, respectively. Thus, we used this parameter to estimate the micropolarity of the hydrophobic bilayer of the vesicles formed. Fig. 3 shows the variation of  $I_1/I_3$  ratio with surfactant concentration. The  $I_1/I_3$  ratio has a value of 1.77 in pH 7.0 PBS (20 mM) in the absence of NaGCh. But the ratio gradually decreased with increasing [NaGCh], which indicates solubilization of Py molecules in the bilayer membrane of vesicles. The limiting minimum value of  $I_1/I_3$  ratio (Table 1) closely matches with that of 2-propanol sol-

**Table 1**  
The self-assembly properties of NaGCh at pH 7.0 PBS (20 mM) at 25 °C. Steady-state fluorescence anisotropy, time-resolved fluorescence lifetime and microviscosity were measured with 0.20 mM (108 µg/mL) NaGCh.

cac (µM)	Micropolarity		$r$	$\tau_f$ (ns)	$\eta_m$ (mPa s)
	$I_1/I_3$	$\pi^*$			
17 ± 1.7	0.90 ± 0.01	0.45	0.253 ± 0.004	5.57 ± 0.1	170 ± 10

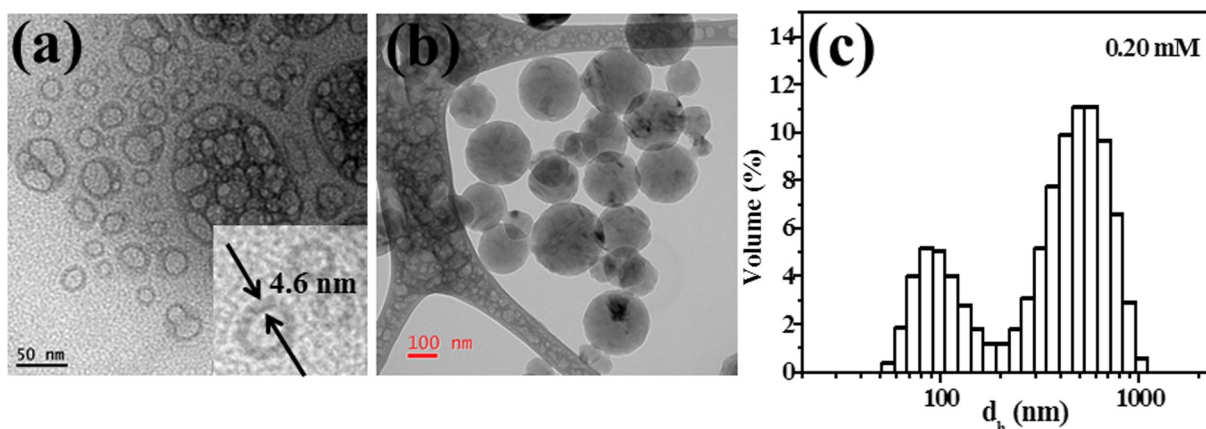


**Fig. 2.** Unstained TEM (a,b) and Cryo-TEM (c) images of the vesicles in 0.20 mM (108 µg/mL) NaGCh dispersion in pH 7.0 buffer; (d) size distribution histogram of the vesicle dispersion at 25 °C.

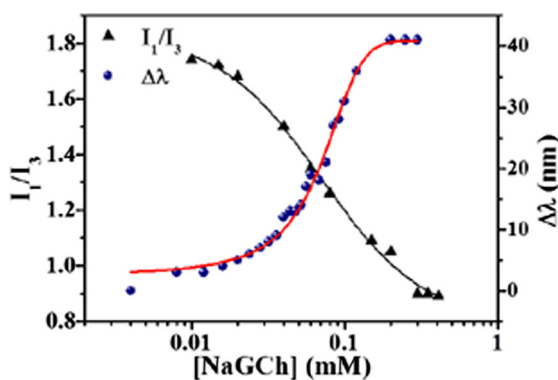


**Fig. 3.** Variation of spectral shift ( $\Delta\lambda$ ) of C153 and  $I_1/I_3$  of Py as a function of [NaGCh] at 25 °C.

vent (0.90) [43]. It should be noted that the vesicles of structurally similar amphiphile NaChol-Ala also showed  $I_1/I_3$  value close to 0.89 [35]. The [NaGCh] value ( $\sim 18$  µM) corresponding to the onset of fall of  $I_1/I_3$  can be taken as the *cac* of the surfactant.

#### 2.1.4. Microviscosity of vesicles

DPH is a fluorescent probe mostly used in the study of fluidity (or rigidity) of lipid bilayer membrane [44,45]. The steady-state fluorescence anisotropy ( $r$ ) value of DPH is a tool for qualitative measurement of the rigidity of its microenvironment in the self-assembled surfactant aggregates. The fluorescence anisotropy of DPH is particularly useful in distinguishing micelles from vesicular structures. For micelles of ionic surfactants,  $r$ -value lies in the range 0.05–0.08 (less rigid environment), while vesicles usually have  $r$ -values  $\geq 0.14$  [46]. In the case of NaGCh, the very high  $r$ -value (Table 1) is reminiscent of the formation of bilayer aggregates with highly rigid and viscous microenvironment.

The rigidity of a microenvironment of the self-assemblies can also be expressed in terms of microviscosity ( $\eta_m$ ). The  $\eta_m$  value was calculated from Debye-Stokes-Einstein relation [47] using

steady-state anisotropy ( $r$ ) and fluorescence lifetime ( $\tau_f$ ) data of DPH probe as presented in Table 1. The  $\tau_f$ -value is similar to that reported for the corresponding  $\alpha$ -alanine derivative, NaChol-Ala, thus confirming solubilization of DPH in a highly nonpolar environment of the vesicle bilayer. The  $\eta_m$  value thus obtained is much higher than those of normal micelles [46].

#### 2.2.5. Stability of vesicles

The above experimental studies demonstrate that NaGCh spontaneously forms spherical SUVs in pH 7.0 PBS at 25 °C. It is well known that spontaneous surfactant self-assemblies are usually reversible molecular self-organization and their physical stability can be altered by external stimuli like temperature, pH, salinity, aging, etc. Therefore, effect of these parameters on vesicle stability was studied. We performed DLS and zeta potential measurements at different pHs and fluorescence anisotropy at different temperatures.

Zeta potential is a measure of the surface charge density of particles in dispersion determines degree of repulsion between adjacent, similarly charged particles. It is one of the fundamental parameters whose magnitude determines colloidal stability. A high  $\zeta$ -potential value (positive or negative) will confer resistance against aggregation and hence high formulation stability and shelf life. When the  $\zeta$ -potential is low, attraction exceeds repulsion and the dispersion will break and flocculate. Therefore, the  $\zeta$ -potential values of NaGCh dispersions at different concentrations were measured. The data are presented in Fig. 4(a). The negative  $\zeta$ -potential suggests that the surface of the vesicular aggregates is negatively charged, as expected. The high numerical values ( $\sim -90$  mV) of  $\zeta$ -potential suggest electrostatic repulsions between carboxylate head groups on the surface and hence higher vesicular stability against flocculation or coagulation.

The stability of the vesicles with pH was studied by DLS and  $\zeta$ -potential measurements at different pHs. As revealed by Fig. 4(b), in the case of NaGCh, the smaller aggregates ( $\sim 100$  nm) become still smaller ( $\sim 60$  nm) while the larger vesicles ( $\sim 420$  nm) tend to grow in size when the pH is lowered from 7.0 to 5.0. Also, the

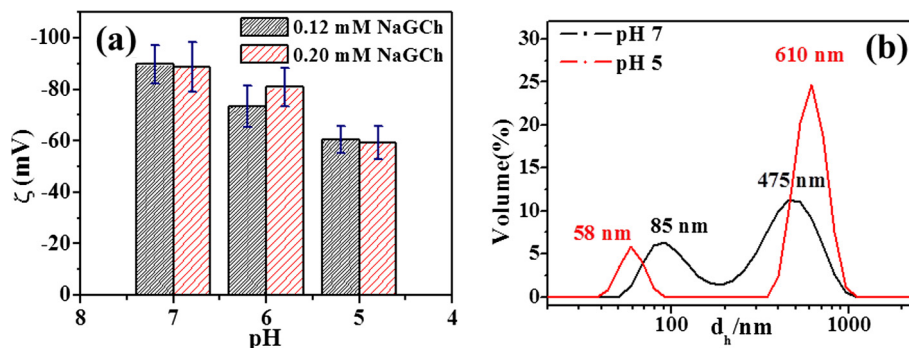


Fig. 4. Effect of pH on (a)  $\zeta$ -potential of the vesicles at 25 °C, and (b) size distribution profiles of vesicles in 0.20 mM (108  $\mu\text{g/mL}$ ) NaGCh dispersion.

relative population of larger vesicles increases with lowering of pH. A plausible explanation is that H-bonding association between head groups  $-\text{COO}^-$  and  $-\text{COOH}$  (partially protonated at pH 5.0) reduces surface charge of the vesicles. This means reduction of electrostatic repulsion among head groups of the surfactant molecules in the vesicles which causes growth of the vesicles. The reduction of surface charge is substantiated by the low  $\zeta$ -potential value at pH 5.0 (see Fig. 4(a)). The pH-induced structural reorganization of the vesicles can be utilized in pH-triggered drug release in drug delivery.

Temperature is an important parameter in ionic surfactant aggregation behavior. Because increase in temperature causes an increase of the degree of counterion ionization and head group repulsions, and disruption of “structured water”, the driving force for aggregation is diminished [48]. In bilayer membranes, increased temperature causes increased membrane fluidity and more water penetration into the bilayer [39,49]. The thermal stability of the vesicles was investigated by recording fluorescence anisotropy ( $r$ ) of the DPH probe in the temperature range of 25–75 °C. Fig. 5(a) depicts the temperature dependence of  $r$  for 0.20 mM (108  $\mu\text{g/mL}$ ) of NaGCh dispersion in pH 7.0 PBS (20 mM). The plot looks like an inverted U shape. The  $r$ -value initially increases with temperature and following a maximum around 37–42 °C, again decreases with further rise in temperature. The initial rise is due to the fact that small rise in temperature facilitates  $-\text{COO}^- \cdots \text{HOOC}-$  H-bonding interaction. However, at elevated temperature, the Chol tails become flexible, making the bilayer more fluid. This may stem from the weakening of hydrophobic interactions caused by thermal motion of the Chol tails at high temperatures. This results in a more hydration (water penetration) of bilayer membrane and hence decreases in  $r$ -value. Such phenomena were also reported elsewhere [50,51].

Investigation of physical stability of vesicles with time is necessary for their practical applications. In order to study the stability of the vesicles with respect to ageing time, the turbidity ( $\tau = 100 - \%T$ ) of the vesicle dispersions was measured at different time intervals over a period of 50 days. Basically, turbidity arises from the scattering of light by the dispersed vesicles, and depends on their size and populations. The results are summarized in Fig. 5 (b). As observed turbidity decreased slightly in the beginning, but remained unchanged thereafter. However, the vesicles overall were observed to be stable.

## 2.2. Entrapment of CUR

CUR was loaded into the vesicle bilayer by a method described under experimental section. In order to show solubilisation of CUR in the vesicle bilayer we performed steady-state fluorescence measurements. For this, CUR-entrapped vesicle dispersion (before dialysis) was diluted with 0.20 mM (108  $\mu\text{g/mL}$ ) vesicle dispersion such that [CUR] becomes 20  $\mu\text{M}$ . After dialysis of this dispersion in a receiver solution containing 0.20 mM NaGCh, fluorescence spectrum (Fig. 6(a)) was measured. For comparison purposes, fluorescence spectrum of a fresh solution of CUR in pure buffer (pH 7) was also recorded. It can be observed that the initial fluorescence intensity of CUR trapped in the vesicles is almost 25 times higher than that for the control. This indicates entrapment of CUR into the hydrophobic region of the vesicles. Also, as evident from Fig. 6(a) there is a huge blue shift (from 547 nm in pure buffer to 500 nm in the presence of NaGCh) of the emission maximum of CUR with respect to that of control.

For determination of EE, the CUR-loaded vesicle dispersion was diluted 100 times with dry methanol and absorbance value was measured at 429 nm using a 1  $\text{cm}^2$  cuvette. The measured absorbance value was 0.109. In a separate experiment, the absorbance

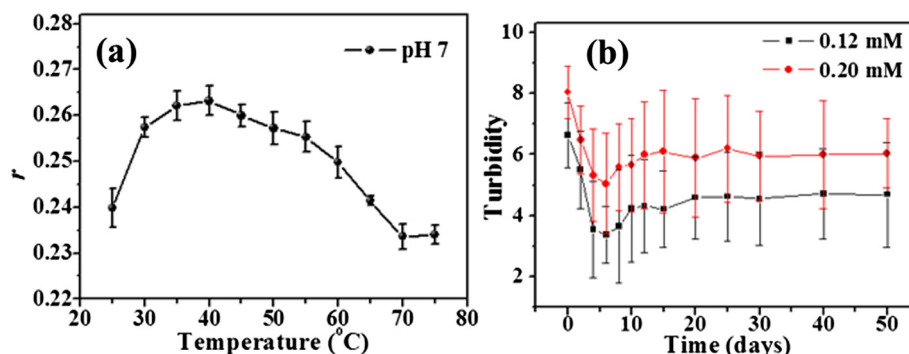
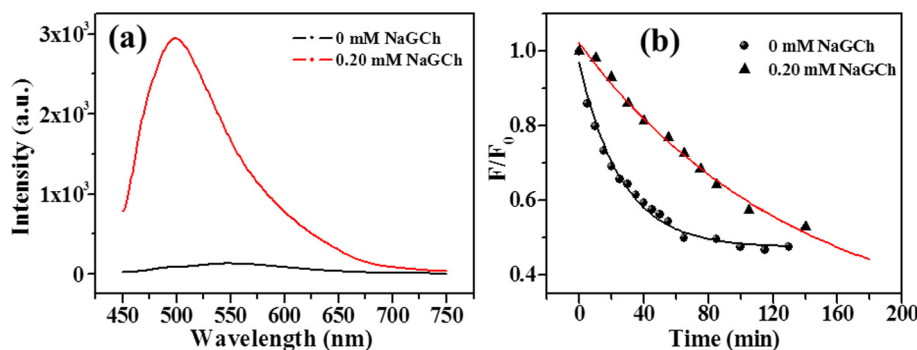


Fig. 5. (a) Effect of temperature on anisotropy of DPH in 0.20 mM (108  $\mu\text{g/mL}$ ) vesicle dispersions; (b) Time variation of turbidity of 0.20 mM (108  $\mu\text{g/mL}$ ) vesicle dispersion in pH 7.0 buffer at 25 °C.



**Fig. 6.** (a) Fluorescence intensity of CUR in the presence and absence of NaGCh. (b) Relative fluorescence intensity ( $F/F_0$ ) versus time plot, showing the time-dependent release of entrapped CUR from the vesicles. The concentrations of NaGCh and CUR before dialysis were 0.20 mM (108  $\mu\text{g}/\text{mL}$ ) and 20  $\mu\text{M}$ , respectively.

values for the CUR solutions of different concentrations (2.7–16.2  $\mu\text{M}$ ) in dry methanol were measured at 429 nm using the same cuvette. The molar extinction coefficient ( $\epsilon = 48,690 \text{ M}^{-1} \text{ cm}^{-1}$ ) was obtained from the calibration plot of absorbance versus [CUR] (see Fig. S6). Thus, the solubility of CUR inside the vesicles of 0.30 mM (161  $\mu\text{g}/\text{mL}$ ) NaGCh was observed to be 0.224 mM (83  $\mu\text{g}/\text{mL}$ ). This means EE of the vesicles is ca. 51%. Similar values of EE for CUR have also been reported by others. Saengkrit et al. have reported that cationic liposome prepared by soybean lecithin showed almost 69% EE for CUR [52]. Also in a most recent study involving chitosan and hyaluronan coated liposomes for pulmonary administration of CUR an EE value of 89–96% was reported for CUR [53]. It should be noted here that liposomes of common lipids, such as phosphatidylcholine and phosphatidylethanolamine solubilize 66 and 51 mol% Chol [54]. Thus the EE (74 mol%) of NaGCh vesicles for CUR is akin to solubility of Chol in liposomes formed by phospholipids.

### 2.3. Stability of CUR-loaded vesicles

The fluorescence spectra of CUR in the absence and presence of NaGCh vesicles were measured at different time intervals and are depicted in Fig. S7. It is evident that the fluorescence intensity of entrapped CUR at 500 nm is reduced to 50% after 145 min in comparison to 73 min in the case of the control. This shows that the entrapment of CUR into the vesicles suppressed its otherwise inevitable degradation in aqueous medium [15,55,56]. In other words, the vesicles protect CUR within its bilayer membrane from rapid degradation.

### 2.4. Cell cytotoxicity assay

The cytotoxicity assay for NaGCh was performed in vitro using MTT assay in the NIH 3T3 cell line. The cytotoxic effect of each treatment is expressed as percentage of cell viability relative to the untreated control cells. The percentage of cell viability is plotted against [NaGCh] in Fig. 7. It is observed that cell viability remained 60% even at a concentration as high as 500  $\mu\text{M}$ . This means that the  $\text{IC}_{50}$  value for the surfactant is  $>500 \mu\text{M}$ . This shows biocompatible nature of NaGCh surfactant.

### 2.5. Cellular uptake study

To investigate the cellular uptake property of vesicles, the cell imaging was performed by treating the MDA-MB-231 cells with CUR-loaded vesicles. The CUR-loaded vesicles were observed to readily internalize into the cells within 3 h of treatment. This is indicated by the bright green fluorescence observed in confocal micrographs (Fig. 8). It is noteworthy that Chol is known to mod-

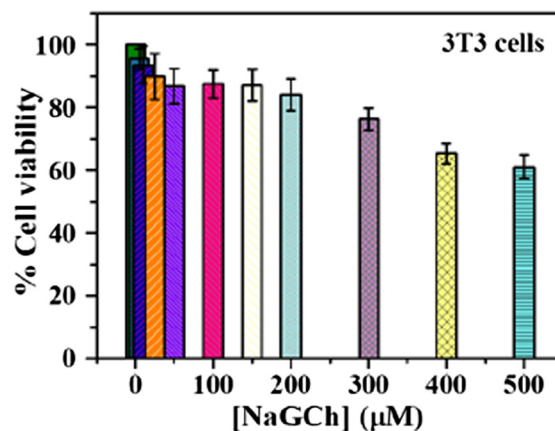


**Fig. 7.** Bar graphs showing results of cytotoxicity assay of NaGCh on NIH 3T3 cells. MTT assay was performed after 4 h of treatment and it was expressed as the percentage of growth with respect to untreated control cells. The data are presented as the mean  $\pm$  SD.

ulate membrane fluidity and hence permeability. The steroidal backbone of NaGCh might have enhanced the rapid permeation of the vesicles into the cells.

## 3. Conclusions

Since the rapid growth of detergency industry is triggered by the rising demand of household, personal care and pharmaceutical products, the last decade has therefore witnessed increasing interest for biofriendly surfactants. Thus, in this work, we have designed and developed a novel biofriendly anionic surfactant NaGCh consisting of two biomolecules Chol and GABA. We have demonstrated spontaneous formation of SUVs by NaGCh surfactant above a very low  $cac$  (17  $\mu\text{M}$ ) in neutral phosphate buffer at room temperature. The vesicle dispersion was found to be very stable at physiological temperature (37  $^{\circ}\text{C}$ ) and pH (7.4). The robust bilayer membrane made these vesicles more stable than liposomes formed by phospholipids. However, the size of the SUVs decreases upon lowering of pH. This phenomenon can be utilized in pH-triggered drug release. Thus in line with the previously reported CUR loading by vesicles [26–29], this work has demonstrated a 207-fold enhancement of aqueous solubility of CUR in dilute dispersion of NaGCh surfactant. Indeed the EE (51%) of these vesicles is much higher than that of liposomes formed by Lipid S75 consisting mainly of phosphatidylcholine, phosphatidylethanolamine and lysophosphatidylcholine [57]. Although the EE of NaGCh vesicles was found to be less than that of vesicles formed by different cyclodextrin amphi-

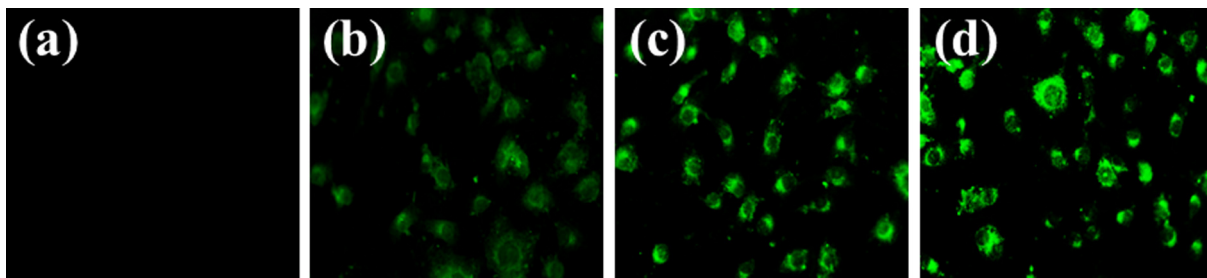


**Fig. 8.** Confocal fluorescence micrographs of MDA-MB-231 cells incubated with CUR-loaded vesicles (0.20 mM, 108  $\mu\text{g}/\text{mL}$ ) for: (a) control, (b) 1 h, (c) 2 h, and (d) 3 h incubation.

philes [29] and soybean lecithin [52], and polymeric nanospheres [19], the NaGCh vesicles have greater shelf-life. Also the entrapment of CUR within vesicle bilayer reduced the hydrolytic degradation of CUR in water. In other words, CUR-loaded vesicle formulation was found to have long shelf-life. The MTT assay showed that the anionic surfactant, NaGCh, was non-cytotoxic to human NIH 3T3 cells. The CUR was successfully delivered in vitro to MDA-MB-231 cells. The steroidal backbone of NaGCh was observed to enhance the permeation of the vesicles into the cells. In fact, liposomes containing cholesterol analogues are known to enhance bioavailability of insulin in oral delivery [58]. These results thus suggest that the spontaneously formed SUVs of NaGCh can have potential applications as pH-triggered release vehicle in delivery of hydrophobic and pharmaceutically-active agents. Further, GABA being a chief inhibitory neurotransmitter [33,34] in the central nervous system and Chol being a ubiquitous component of cell membrane [31], the SUVs formed by NaGCh are expected to overcome the blood-brain barrier (BBB). In other words, the NaGCh vesicles can have potential application in drug delivery to brain for treatment of diseases like Alzheimer's and brain cancer.

## 4. Materials and methods

### 4.1. Materials

Cholesteryl chloroformate ( $\sim 95\%$ ),  $\gamma$ -amino butyric acid ( $\geq 99\%$ ) and curcumin (CUR,  $\geq 94\%$ ) were purchased from Sigma-Aldrich (Bangalore, India) and used without further purification. Fluorescence probes, N-phenyl-1-naphthalamine (NPN, 98%), pyrene (Py, 98%), coumarin-153 (C153, 99%), and 1,6-diphenyl-1,3,5-hexatriene (DPH, 98%) were also purchased from Sigma-Aldrich (Bangalore, India) and were purified by recrystallization.  $\text{CDCl}_3$  (Cambridge Isotope Laboratory, USA) was used as a solvent for NMR. The surfactant NaGCh was synthesized in our laboratory. The details of synthetic procedure and spectroscopic data for chemical identification are given under “Supporting Information” (SI).

### 4.2. Methods

#### 4.2.1. General instrumentation

$^1\text{H}$ - and  $^{13}\text{C}$ -NMR spectra were recorded on an AVANCE DAX-400 (Bruker, Sweden) 400 MHz NMR spectrometer. A Perkin Elmer RX1 FTIR spectrometer (USA) was used for recording FT-IR spectra. Melting point was determined using InstInd (Kolkata) melting point apparatus with open capillaries. Turbidity measurements employed a Shimadzu (Model 1601, Japan) UV-Vis spectrophotometer. The percentage transmittance (%T) of surfactant solutions was measured at 400 nm at different time intervals. Turbidity ( $\tau$ ) was calculated using the relation,  $\tau = 100 - \%T$ . The pH measure-

ments were done with digital pH meter (Model 111, India) using a glass electrode. Aqueous phosphate buffers used for the solution studies were prepared by mixing  $\text{NaH}_2\text{PO}_4$  (927  $\mu\text{g}/\text{mL}$ ) and  $\text{Na}_2\text{-HPO}_4$  (1741  $\mu\text{g}/\text{mL}$ ) in Milli-Q water (18.2 M $\Omega$ ). All measurements were carried out at 25  $^\circ\text{C}$  unless otherwise mentioned.

#### 4.2.2. Steady-state fluorescence measurements

The fluorescence emission spectra of NPN and C153 probes were recorded on a Hitachi (F-7000, Japan) spectrophotometer. For fluorometric titration, the final concentration of NPN and C153 was 1  $\mu\text{M}$ . The solutions containing NPN and C153 were excited at 340 and 420 nm, respectively.

#### 4.2.3. Fluorescence anisotropy measurements

A Perkin Elmer LS-55 luminescence spectrometer (USA) was used to measure the steady-state fluorescence anisotropy ( $r$ ) of DPH in the presence of the surfactants. The instrument is equipped with a polarization accessory that uses the L-format instrumental configuration and a thermostated and magnetically stirred cell housing that allowed temperature control. The anisotropy was calculated employing the equation [59]:

$$r = (I_{VV} - GI_{VH}) / (I_{VV} + 2GI_{VH}) \quad (2)$$

where  $I_{VV}$  and  $I_{VH}$  are the fluorescence intensities polarized parallel and perpendicular to the excitation light, and  $G (= I_{HV}/I_{HH})$  is the instrumental grating factor. The software supplied by the manufacturer automatically determined the  $G$ -factor and  $r$ . For each measurement, the  $r$ -value was recorded over an integration time of 10 s. For each sample, an average of five readings was accepted as the value of  $r$ . A stock solution of 1 mM DPH was prepared in super dry methanol. Aliquots of this stock solution were added to the surfactant solutions so that the final concentration of the probe was  $\sim 1 \mu\text{M}$ . The anisotropy measurements were carried out at different surfactant concentrations in the temperature range 25–75  $^\circ\text{C}$ . Before measurement started, each solution was equilibrated for 10 min at the experimental temperature. The sample was excited at 350 nm and the emission intensity was followed at 450 nm using excitation and emission slit width of 2.5 nm and 2.5–10.0 nm, respectively. A 430 nm cut-off filter was placed in the emission beam to eliminate the effect of scattered radiation.

#### 4.2.4. Time-resolved fluorescence measurements

An Easylife<sup>TM</sup> X (Optical Building Blocks Corporation, USA) time-resolved instrument was used to measure the fluorescence lifetime of DPH probe. The light source was a 380 nm diode laser. The time-resolved decay curves were analyzed by single exponential or bi-exponential iterative fitting program. The best fit was judged by the  $\chi^2$  value (0.8–1.2) and by the randomness of residual plot.

#### 4.2.5. Determination of microviscosity

The rigidity or fluidity of the microenvironment of the self-assemblies was measured by determination of the microviscosity ( $\eta_m$ ) using DPH probe. The  $\eta_m$  was calculated from the values of  $r$  and rotational correlation time ( $\tau_R$ ) of DPH probe using Debye–Stokes–Einstein relation [47]:

$$\eta_m = kT\tau_R/v_h \quad (3)$$

where  $v_h$  is the hydrodynamic volume ( $313 \text{ \AA}^3$ ) [46] of the DPH molecule. The  $\tau_R$  was calculated using Perrin's equation [59]:

$$\tau_R = \tau_f(r_o/r - 1)^{-1} \quad (4)$$

where  $r_o$  ( $= 0.362$ ) [60] and  $\tau_f$  are the steady-state fluorescence anisotropy of DPH in a highly viscous solvent and measured fluorescence lifetime of DPH in surfactant solution, respectively.

#### 4.2.6. Dynamic light scattering (DLS)

The DLS technique was used to measure the size distribution of the aggregates formed in aqueous dispersion of NaGCh. The DLS measurements employed a Zetasizer Nano ZS (Malvern Instrument Lab., Malvern, UK) equipped with a He–Ne laser working at 4 mW ( $\lambda_o = 632.8 \text{ nm}$ ). Each sample was allowed to equilibrate inside the DLS optical system chamber for 5 min prior to the start of the measurement. All measurements were performed at  $25 \pm 0.1 \text{ }^\circ\text{C}$ . The scattering intensity was measured at  $173^\circ$  to the incident beam. The instrument automatically performed several runs in order to produce a monomodal or multimodal size distribution profile.

#### 4.2.7. Zeta potential measurements

To evaluate the surface charge density of the vesicles, zeta potential was measured on a Zetasizer Nano ZS (Malvern Instrument Lab., Malvern, UK) instrument using folded capillary cell. The reported value is the average of three readings. In principle, the Zetasizer Nano instrument calculates the zeta potential by determining the electrophoretic mobility and then applying the Henry equation. The electrophoretic mobility is obtained by performing an electrophoresis experiment on the sample and measuring the velocity of the particles using laser Doppler velocimetry (LDV). The Henry equation [61] is

$$U_E = \frac{2\varepsilon\zeta f(ka)}{3\eta} \quad (5)$$

where  $U_E$  is electrophoretic mobility,  $\varepsilon$  is dielectric constant,  $\zeta$  is Zeta potential,  $\eta$  is viscosity and  $f(ka)$  is Henry function. Two values (either 1.5 or 1.0) are generally used as approximations for the  $f(ka)$  determination. For small particles in low dielectric constant media,  $f(ka)$  is 1.0. This is referred to as the Huckel approximation. Non-aqueous measurements generally use the Huckel approximation. For aqueous samples with moderate electrolyte concentration, the Smoluchowski approximation is used and  $f(ka) = 1.5$ .

#### 4.2.8. Transmission electron microscopy (TEM)

The morphology of the aggregates was visualized with a transmission electron microscope (FEI-TECNAI G2 20S-TWIN, FEI, USA) operating at an accelerating voltage of 120 kV. Using a fresh syringe, a  $2 \mu\text{L}$  tiny droplet of NaGCh dispersion was cast on to a 400 mesh size carbon-coated copper grid, and allowed to stand for 1 min, and the grid was air-dried overnight before measurement.

#### 4.2.9. Cryo-High resolution transmission electron microscopy (Cryo-HRTEM)

Cryo-HRTEM imaging was performed on a JEM-2100 F transmission electron microscope (JEOL, USA) equipped with a semi-automated plunge freezing instrument (Cp3 Cryoplunge™ 3,

Gatan, USA) used for the preparation of frozen hydrated specimens. The specimen grid clamped between the tines of plunging tweezers and containing  $5 \mu\text{L}$  of NaGCh dispersion was rapidly plunged into a temperature-monitored ethane bath maintained at liquid nitrogen temperature to prevent the formation of ice crystals. A liquid nitrogen workstation, with a remote fill funnel and two removable covers, maintained the temperature of the liquid ethane vessel. The specimen grid was then be moved to a cryo workstation and then into a cryo holder followed by imaging.

#### 4.2.10. Entrapment of curcumin

As the vesicle bilayer is observed to be much less polar, it is expected that hydrophobic drugs such as CUR can be solubilized within vesicle bilayer membrane. CUR was entrapped into the vesicles by solvent evaporation method [62]. To evaluate the maximum solubilization of CUR into the vesicles, NaGCh (1.62 mg) and excess CUR (5 mg) and dry methanol (10 mL) were taken in a 15-mL screw capped vial, and the mixture was stirred magnetically overnight in the darkness. Next, methanol was evaporated in the air. To it was added 10 mL of serum-free sterilized PBS (pH 7.4). The mixture was vortexed for 15 min followed by centrifugation at 3000 rpm for 10 min. The supernatant was collected and was then dialyzed for 30 min, using an ultra-filtration cellulose acetate membrane with pore size of 1000 Da MWCO to remove the free CUR (unentrapped in the vesicles). The receiving medium was 0.30 mM NaGCh ( $\sim 220 \text{ mL}$ ,  $161 \mu\text{g/mL}$ ). The dialyzed solution was further subjected to syringe filtration using nitrocellulose membrane (pore size  $0.22 \mu\text{m}$ , diameter 25 mm). The resulting solution was used for spectroscopic and biological assays. The entrapment efficiency (EE) of the vesicles was calculated from the equation:

$$EE = (\text{Mass of CUR entrapped}/\text{Mass of NaGCh}) \times 100\% \quad (6)$$

#### 4.2.11. Cytotoxicity assay

The cytotoxicity assay of NaGCh in vitro was measured using the MTT (3-(4,5-dimethylthiazol-2-yl)-2,5-diphenyltetrazolium bromide, a yellow tetrazole) assay on the normal cells (NIH 3T3). The cells growing in the log phase were seeded into two 96-well cell-culture plate at  $1 \times 10^4$  cells/mL. Different concentrations of NaGCh were added into the wells with an equal volume of incomplete DMEM medium in the control wells. The cells were then incubated for 48 h at  $37 \text{ }^\circ\text{C}$  in 5%  $\text{CO}_2$ . Thereafter, fresh incomplete DMEM medium containing  $0.40 \text{ mg mL}^{-1}$  of MTT was added to the 95 well plates and incubated for 4 h at  $37 \text{ }^\circ\text{C}$  in 5%  $\text{CO}_2$ . Formazan crystals thus formed were dissolved in DMSO after decanting the earlier media and the absorbance was recorded at 595 nm [63].

#### 4.2.12. Cellular uptake study

The cells ( $1 \times 10^3$  cells/mL) were seeded on coverslips in DMEM medium. After 24 h cells were treated with CUR-loaded vesicles and then incubated for 3 h. Cells were fixed in 3.7% paraformaldehyde. The slides were washed again in PBST twice for 10 min and mounted with D.P.X mountant. Fluorescence images were acquired using a Zeiss Observer confocal fluorescence microscope (Germany) after 1, 2 and 3 h of incubation.

#### 4.2.13. Software and statistical data analysis

All statistical analyses were performed by OriginPro8 and Instat softwares (La Jolla, CA, USA). Measurements were done in replicates to check the reproducibility of results. Average values and standard deviation (SD) were calculated and the results were represented as mean  $\pm$  SD.

## Acknowledgments

The authors acknowledge Indian Institute of Technology Kharagpur for support of this work. D.B. thanks Indian Institute of Technology Kharagpur and Y.R. thanks DST-INSPIRE (IF130658) for research fellowships. We acknowledge Prof. D. Dhara, Department of Chemistry for DLS and zeta potential measurements.

## Conflict of interest

The authors declare no competing financial interests.

## Appendix A. Supplementary material

Supplementary data (details of synthetic procedure, FT-IR, <sup>1</sup>H-NMR, and <sup>13</sup>C-NMR spectra and chemical identification of the synthesized surfactant, representative fluorescence emission spectra of NPN and C153) associated with this article can be found in the online version. Supplementary data associated with this article can be found, in the online version, at <http://dx.doi.org/10.1016/j.jcis.2017.07.108>.

## References

- [1] National Center for Health Statistics (US). (2016). Health, United States, 2015: with Special Feature on Racial and Ethnic Health Disparities.
- [2] M. Bethesda, A Closer Look at Ayurvedic Medicine. Focus on Complementary and Alternative Medicine, National Center for Complementary and Alternative Medicine, US National Institutes of Health, (2006).
- [3] R.K. Maheshwari, A.K. Singh, J. Gaddipati, R.C. Srimal, Multiple biological activities of curcumin: a short review, *Life Sci.* 78 (2006) 2081–2087.
- [4] P.S. Negi, G.K. Jayaprakasha, L. Jagan Mohan Rao, K. Sakariah, Antibacterial activity of turmeric oil: a byproduct from curcumin manufacture, *J. Agric. Food Chem.* 47 (1999) 4297–4300.
- [5] O.P. Sharma, Antioxidant activity of curcumin and related compounds, *Biochem. Pharmacol.* 25 (1976) 1811–1812.
- [6] R.C. Srimal, B.N. Dhawan, Pharmacology of diferuloyl methane (curcumin), a non-steroidal anti-inflammatory agent, *J. Pharm. Pharmacol.* 25 (1973) 447–452.
- [7] F. Yang, G.P. Lim, A.N. Begum, O.J. Ubeda, M.R. Simmons, S.S. Ambegaokar, P.P. Chen, R. Kayed, C.G. Glabe, S.A. Frautschy, G.M. Cole, Curcumin inhibits formation of amyloid beta oligomers and fibrils, binds plaques, and reduces amyloid in vivo, *J. Biol. Chem.* 280 (2005) 5892–5901.
- [8] R.A. Sharma, A.J. Gescher, W.P. Steward, Curcumin: the story So Far, *Eur. J. Cancer* 41 (2005) 1955–1968.
- [9] R. Kuttan, P. Bhanumathy, K. Nirmala, M.C. George, Potential anticancer activity of turmeric (*curcuma longa*), *Cancer Lett.* 29 (1985) 197–202.
- [10] S. Reuter, J. Charlet, T. Juncker, M.H. Teiten, M. Dicato, M. Diederich, Effect of curcumin on nuclear factor kappaB signaling pathways in human chronic myelogenous K562 leukemia cells, *Ann. N.Y. Acad. Sci.* 1171 (2009) 436–447.
- [11] S. Anuchapreeda, P. Leechanachai, M.M. Smith, S.V. Ambudkar, P.N. Limtrakul, Modulation of P-glycoprotein expression and function by curcumin in multidrug-resistant human KB cells, *Biochem. Pharmacol.* 64 (2002) 573–582.
- [12] S. Ganta, M. Amiji, Co-administration of paclitaxel and curcumin in nanoemulsion formulations to overcome multidrug resistance in tumor cells, *Mol. Pharm.* 6 (2009) 928–939.
- [13] W. Li-Xian, X. Jian-Hua, W. Guo-Hua, C. Yuan-Zhong, Inhibitory effect of curcumin on proliferation of k562 cells involves down-regulation of p210<sup>bcr/abl</sup>-initiated ras signal transduction pathway, *Acta Pharmacol. Sin.* 24 (2003) 1155–1160.
- [14] <http://clinicaltrials.gov/ct2/results?term=curcumin>. (ClinicalTrials.gov, a service of the U.S. National Institutes of Health, is a registry and results database of publicly and privately supported clinical studies of human participants conducted around the world.) Accessed on 12th Jan 2017.
- [15] H.H. Tønnesen, J. Karlsen, Studies on curcumin and curcuminoids. VI. kinetics of curcumin degradation in aqueous solution, *Z. Lebensm. Unters. Forsch.* 180 (1985) 402–404.
- [16] H.H. Tønnesen, J. Karlsen, G.B. van Henegouwen, Studies on curcumin and curcuminoids. VIII. photochemical stability of curcumin, *Z. Lebensm. Unters. Forsch.* 183 (1986) 116–122.
- [17] H.H. Tønnesen, Solubility, chemical and photochemical stability of curcumin in surfactant solutions. studies of curcumin and curcuminoids, XXVIII, *Pharmazie* 57 (2002) 820–824.
- [18] P. Anand, A.B. Kunnammakkara, R.A. Newman, B.B. Aggarwal, Bioavailability of curcumin: problems and promises, *Mol. Pharm.* 4 (2007) 807–818.
- [19] A. Mukerjee, J.K. Vishwanatha, Formulation, characterization and evaluation of curcumin-loaded PLGA nanospheres for cancer therapy, *Anticancer Res.* 29 (2009) 3867–3875.
- [20] M. Gou, K. Men, H. Shi, M. Xiang, J. Zhang, J. Song, J. Long, Y. Wan, F. Luo, X. Zhao, Z. Qian, Curcumin-loaded biodegradable polymeric micelles for colon cancer therapy in vitro and in vivo, *Nanoscale* 3 (2011) 1558–1567.
- [21] L. Li, F.S. Braiteh, R. Kurzrock, Liposome-encapsulated curcumin: in vitro and in vivo effects on proliferation, apoptosis, signaling, and angiogenesis, *Cancer* 104 (2005) 1322–1331.
- [22] M.H. Lee, H.Y. Lin, H.C. Chen, J.L. Thomas, Ultrasound mediates the release of curcumin from microemulsions, *Langmuir* 24 (2008) 1707–1713.
- [23] P.P. Dandekar, R. Jain, S. Patil, R. Dhupal, D. Tiwari, S. Sharma, G. Vanage, V. Patravale, Curcumin-loaded hydrogel nanoparticles: application in anti-malarial therapy and toxicological evaluation, *J. Pharm. Sci.* 99 (2010) 4992–5010.
- [24] W. Mehnert, K. Mäder, Solid lipid nanoparticles: production, characterization and applications, *Adv. Drug Deliv. Rev.* 47 (2001) 165–196.
- [25] H. Tang, C.J. Murphy, B. Zhang, Y. Shen, E.A. Van Kirk, W.J. Murdoch, M. Radosz, Curcumin polymers as anticancer conjugates, *Biomaterials* 31 (2010) 7139–7149.
- [26] A. Kumar, G. Kaur, S.K. Kansal, G.R. Chaudhary, S.K. Mehta, Enhanced solubilization of curcumin in mixed surfactant vesicles, *Food Chem.* 199 (2016) 660–666.
- [27] C. Liu, H. Huang, In vitro anti-propionibacterium activity by curcumin containing vesicle system, *Chem. Pharm. Bull.* 61 (2013) 419–425.
- [28] S. Zupančič, P. Kocbek, M.G. Zariwala, D. Renshaw, M.O. Gul, Z. Elsaid, K.M.G. Taylor, S. Somavarapu, Design and development of novel mitochondrial targeted nanocarriers DQAsomes for curcumin inhalation, *Mol. Pharm.* 11 (2014) 2334–2345.
- [29] M. Ma, T. Suna, P. Xing, Z. Li, S. Li, J. Su, X. Chu, A. Hao, A, supramolecular curcumin vesicle and its application in controlling curcumin release, *Colloids Surf., A* 459 (2014) 157–165.
- [30] M.M. Yallapu, M. Jaggi, S.C. Chauhan, Curcumin nanoformulations: a future nanomedicine for cancer, *Drug Discov. Today* 17 (2012) 71–80.
- [31] P.L. Yeagle, Cholesterol and the cell membrane, *Biochim. Biophys. Acta* 822 (1985) 267–287.
- [32] F.C. Steward, J.F. Thompson, C.E. Dent,  $\gamma$ -Aminobutyric Acid: a constituent of the potato tuber?, *Science* 110 (1949) 439–440.
- [33] A.W. Bown, B.J. Shelp, The metabolism and functions of  $\gamma$ -aminobutyric acid, *Plant Physiol.* 115 (1997) 1–5.
- [34] C.F. Baxter, The Nature of  $\gamma$ -Aminobutyric Acid, In *Handbook of Neurochemistry. Volume III: Metabolic Reactions in the Nervous System*; Lajtha, A., Ed.; Plenum Press: New York (1970) pp 289–353 Chapter 9.
- [35] D. Bajani, P. Laskar, J. Dey, Spontaneously formed robust steroidal vesicles: physicochemical characterization and interaction with HSA, *J. Phys. Chem. B* 118 (2014) 4561–4570.
- [36] A. Ghosh, J. Dey, Effect of hydrogen bonding on the physicochemical properties and bilayer self-assembly formation of N-(2-hydroxydodecyl)-L-alanine in aqueous solution, *Langmuir* 24 (2008) 6018–6026.
- [37] D. Khatua, S. Ghosh, J. Dey, G. Ghosh, V.K. Aswal, Physicochemical properties and microstructure formation of the surfactant mixtures of sodium N-(2-(n-dodecylamino) ethanoyl)-L-alanine and SDS in aqueous solutions, *J. Phys. Chem. B* 112 (2008) 5374–5380.
- [38] A. Ghosh, S. Shrivastava, J. Dey, Concentration and pH-dependent aggregation behavior of an L-histidine based amphiphile in aqueous solution, *Chem. Phys. Lipids* 163 (2010) 561–568.
- [39] T. Patra, S. Ghosh, J. Dey, Spontaneous formation of pH-sensitive, stable vesicles in aqueous solution of N-[4-n-octyloxybenzoyl]-L-histidine, *Soft Matter* 6 (2010) 3669–3679.
- [40] J. Dey, S. Shrivastava, Physicochemical characterization and self-assembly studies on cationic surfactants bearing mPEG Tail, *Langmuir* 28 (2012) 17247–17255.
- [41] S. Roy, J. Dey, Effect of Hydrogen-bonding interactions on the self-assembly formation of sodium N-(11-acrylamidoundecanoyl)-L-serinate, L-asparaginate, and L-glutamate in aqueous solution, *J. Colloid Interface Sci.* 307 (2007) 229–234.
- [42] M.L. Horng, J.A. Gardecki, A. Papazyan, M. Maroncelli, Subpicosecond measurements of polar solvation dynamics: coumarin 153 revisited, *J. Phys. Chem.* 99 (1995) 17311–17337.
- [43] K. Kalyanasundaram, J.K. Thomas, Environmental effects on vibronic band intensities in pyrene monomer fluorescence and their application in studies of micellar systems, *J. Am. Chem. Soc.* 99 (1977) 2039–2044.
- [44] G. Weber, M. Shinitzky, A.C. Dianoux, C. Gitler, Microviscosity and order in the hydrocarbon region of micelles and membranes determined with fluorescent probes I. Synthetic Micelles, *Biochemistry* 10 (1971) 2106–2113.
- [45] M. Shinitzky, I. Yuli, Lipid fluidity at the submacroscopic level: determination by fluorescence polarization, *Chem. Phys. Lipids* 30 (1982) 261–282.
- [46] S. Roy, A. Mohanty, J. Dey, Microviscosity of bilayer membranes of some n-acylamino acid surfactants determined by fluorescence probe method, *Chem. Phys. Lett.* 414 (2005) 23–27.
- [47] P. Debye, *Polar Molecules*, Dover, New York, 1929.
- [48] S.S. Shah, E. Rehman, Effect of Temperature and Aprotic Solvents on the CMC of Sodium Dodecyl Sulfate, in: H. Kleeberg (Ed.), *Interactions of Water in Ionic and Nonionic Hydrates*, Springer, Berlin, 1987, pp. 251–255.
- [49] W.V. Kraske, D.B. Mountcastle, Effects of cholesterol and temperature on the permeability of dimyristoylphosphatidylcholine bilayers near the chain melting phase transition, *BBA-Biomembranes* 1514 (2001) 159–164.
- [50] G. Caracciolo, D. Pozzi, R. Caminiti, C. Marianecchi, S. Moglioni, M. Carafa, H. Amenitsch, Effect of hydration on the structure of solid-supported niosomal

- membranes investigated by in situ energy dispersive x-ray diffraction, *Chem. Phys. Lett.* 462 (2008) 307–312.
- [51] D. Pozzi, R. Caminiti, C. Marianecci, M. Carafa, E. Santucci, S.C. De Sanctis, G. Caracciolo, Effect of cholesterol on the formation and hydration behavior of solid-supported niosomal membranes, *Langmuir* 26 (2010) 2268–2273.
- [52] N. Saengkrit, S. Saesoo, W. Srinuanchai, S. Phunpee, U.R. Ruktanonchai, Influence of curcumin-loaded cationic liposome on anticancer activity for cervical cancer therapy, *Colloids Surf., B* 114 (2014) 349–356.
- [53] M. Manconi, M.L. Manca, D. Valenti, E. Escibano, H. Hillaireau, A.M. Fadda, E. Fattal, Chitosan and hyaluronan coated liposomes for pulmonary administration of curcumin, *Int. J. Pharm.* 525 (2017) 203–210.
- [54] J. Huang, J.T. Buboltz, G.W. Feigenson, Maximum solubility of cholesterol in phosphatidylcholine and phosphatidylethanolamine bilayers, *BBA-Biomembranes* 1417 (1999) 89–100.
- [55] J.K. Lin, M.H. Pan, S.Y. Lin-Shiau, Recent studies on the biofunctions and biotransformations of curcumin, *Biofactors* 13 (2000) 153–158.
- [56] Y.J. Wang, M.H. Pan, A.L. Cheng, L.I. Lin, Y.S. Ho, C.Y. Hsieh, J.K. Lin, Stability of curcumin in buffer solutions and characterization of its degradation products, *J. Pharm. Biomed. Anal.* 15 (1997) 1867–1876.
- [57] C. Cheng, S. Peng, Z. Li, L. Zou, W. Liu, C. Liu, Improved bioavailability of curcumin in liposomes prepared using a ph-driven, organic solvent-free, Easily Scalable Process, *RSC Adv.* 7 (2017) 25978–25986.
- [58] M. Cui, W. Wu, L. Hovgaard, Y. Lu, D. Chen, J. Qi, Liposomes containing cholesterol analogues of botanical origin as drug delivery systems to enhance the oral absorption of insulin, *Int. J. Pharm.* 489 (2015) 277–284.
- [59] J.R. Lakowicz, *Principles of Fluorescence Spectroscopy*, Plenum Press, New York, 1983.
- [60] M. Shinitzky, Y. Barenholz, Dynamics of the hydrocarbon layer in liposomes of lecithin and sphingomyelin containing dicetylphosphate, *J. Biol. Chem.* 249 (1974) 2652–2657.
- [61] D.C. Henry, The cataphoresis of suspended particles. part I. the equation of cataphoresis, *Proc. R. Soc. A* 133 (1931) 106–129.
- [62] R.R.C. New, *Liposomes—A Practical Approach*, IRL Press at Oxford University Press, Oxford, New York, Tokyo, 1990.
- [63] I. Pal, K.K. Dey, M. Chaurasia, S. Parida, S. Das, Y. Rajesh, K. Sharma, T. Chowdhury, M. Mandal, Cooperative effect of BI-69A11 and celecoxib enhances radiosensitization by modulating DNA Damage repair in colon carcinoma, *Tumor Biol.* 37 (2016) 6389–6402.